RSC Advances

PAPER

View Article Online
View Journal | View Issue

Cite this: *RSC Adv.*, 2020, **10**, 26433

Theoretical investigation of the reaction mechanisms and kinetics of $CFCl_2CH_2O_2$ and ClO in the atmosphere†

Yunju Zhang *[a] and Bing He[b]

The reaction between $CFCl_2CH_2O_2$ radicals and ClO was studied using the B3LYP and CCSD(T) methods associated with the 6-311++G(d,p) and cc-pVTZ basis sets, and subsequently RRKM-TST theory was used to predict the thermal rate constants and product distributions. On the singlet PES, the dominant reaction is the addition of the ClO oxygen atom to the terminal-O of $CFCl_2CH_2O_2$ to generate adduct IM1 ($CFCl_2CH_2OOOCl$), and then dissociation to final products **P1** ($CFCl_2CHO + HO_2 + Cl$) occurs. RRKM theory is employed to calculate the overall and individual rate constants over a wide range of temperatures and pressures. It is predicted that the collision-stabilized **IM1** ($CFCl_2CH_2OOOCl$) dominates the reaction at 200–500 K (accounting for about 60–100%) and the dominant products are **P1** ($CFCl_2CHO + HO_2 + Cl$). The yields of the other products are very low and insignificant for the title reaction. The total rate constants exhibit typical "falloff" behavior. The pathways on the triplet PES are less competitive than that on the singlet PES. The calculated overall rate constants are in good agreement with the experimental data. The atmospheric lifetime of $CFCl_2CH_2O_2$ in ClO is around 2.04 h. TD-DFT calculations imply that **IM1** ($CFCl_2CH_2OOOCl$), **IM2** ($CFCl_2CH_2OOClO$) and **IM3** ($CFCl_2CH_2OClO_2$) will photolyze under sunlight.

Received 28th May 2020
Accepted 19th June 2020

DOI: 10.1039/d0ra04707d

rsc.li/rsc-advances

1. Introduction

The detrimental influence of CFCs (chlorofluorocarbons) on the ozonosphere and stratosphere resulted in international agreement that the manufacturing of these chemical compounds would be discontinued by January 1996.[1,2] HCFCs (hydrochlorofluorocarbons) are the suggested alternatives to CFCs since they are relatively environmentally benign. When HCFCs are released into the troposphere, they could react with OH radicals to generate haloalkyl radicals, which subsequently react with O_2 to form peroxy radicals in low altitude atmosphere.[1,2] With HCFC-14lb ($CFCl_2CH_3$) as a substitute for CFC, the reactions are as follows:

$$CFCl_2CH_3 + OH \rightarrow CFCl_2CH_2 + H_2O$$

$$CFCl_2CH_2 + O_2 + M \rightarrow CFCl_2CH_2O_2 + M$$

To assess the atmospheric effects of $CFCl_2CH_3$, it is necessary to study the peroxy radical ($CFCl_2CH_2O_2$) generated by the atmospheric reaction of $CFCl_2CH_3$. The possible degradation mechanism of the peroxy radicals includes self-reactions[3–5] and reactions with free radicals, *i.e.* Cl, ClO, NO, HO_2 and CH_3O_2.[6–11] It is well-known that the ClO radical is the most abundant reactive halogen species in the atmosphere. It is of great atmospheric importance due to its ability to destroy ozone. Based on the catalytic cycle, ClO plays an important role in the generation of the Antarctic "ozone hole", especially in the production of the South ozone hole.[12] The generation and photolysis for the dipolymer of ClO (ClOOCl) are critical for the chemical reaction. According to the statistics, this cycle contributed to about 70% of the damage to the Antarctic ozone.[13] However, previous research indicated that this gas phase chemistry alone does not result in ozone depletion due to the ozone depletion by chlorine-catalyzed reactions.[14] Therefore, the reaction of ClO with $CFCl_2CH_2O_2$ is a quite significant chemical reaction, which was only studied by one earlier experiment. In 1977, Wu and Carr[7] studied the kinetics of the reaction between ClO and $CFCl_2CH_2O_2$ by employing time-resolved mass spectrometry and a UV flash photolysis technique and measured the rate constant at 253–321 K and 4–60 torr. The obtained rate constant was $(6.0 \pm 0.7) \times 10^{-12}$ cm^3 per molecule per s at 298 K. Moreover, although studies have involved the $CFCl_2CH_2O_2$ + ClO reaction,[15] there have been no theoretical investigations into the ClO + $CFCl_2CH_2O_2$ reaction, which may indicate the degradation of ClO with $CFCl_2CH_2O_2$, affecting the stratospheric ozone consumption, which may

[a]*Key Laboratory of Photoinduced Functional Materials, Mianyang Normal University, Mianyang 621000, PR China. E-mail: zhangyj010@nenu.edu.cn; Fax: +86 816 2200819; Tel: +86 816 2200064*

[b]*College of Chemistry and Life Science, Institute of Functional Molecules, Chengdu Normal University, Chengdu, Sichuan 611130, PR China*

† Electronic supplementary information (ESI) available. See DOI: 10.1039/d0ra04707d

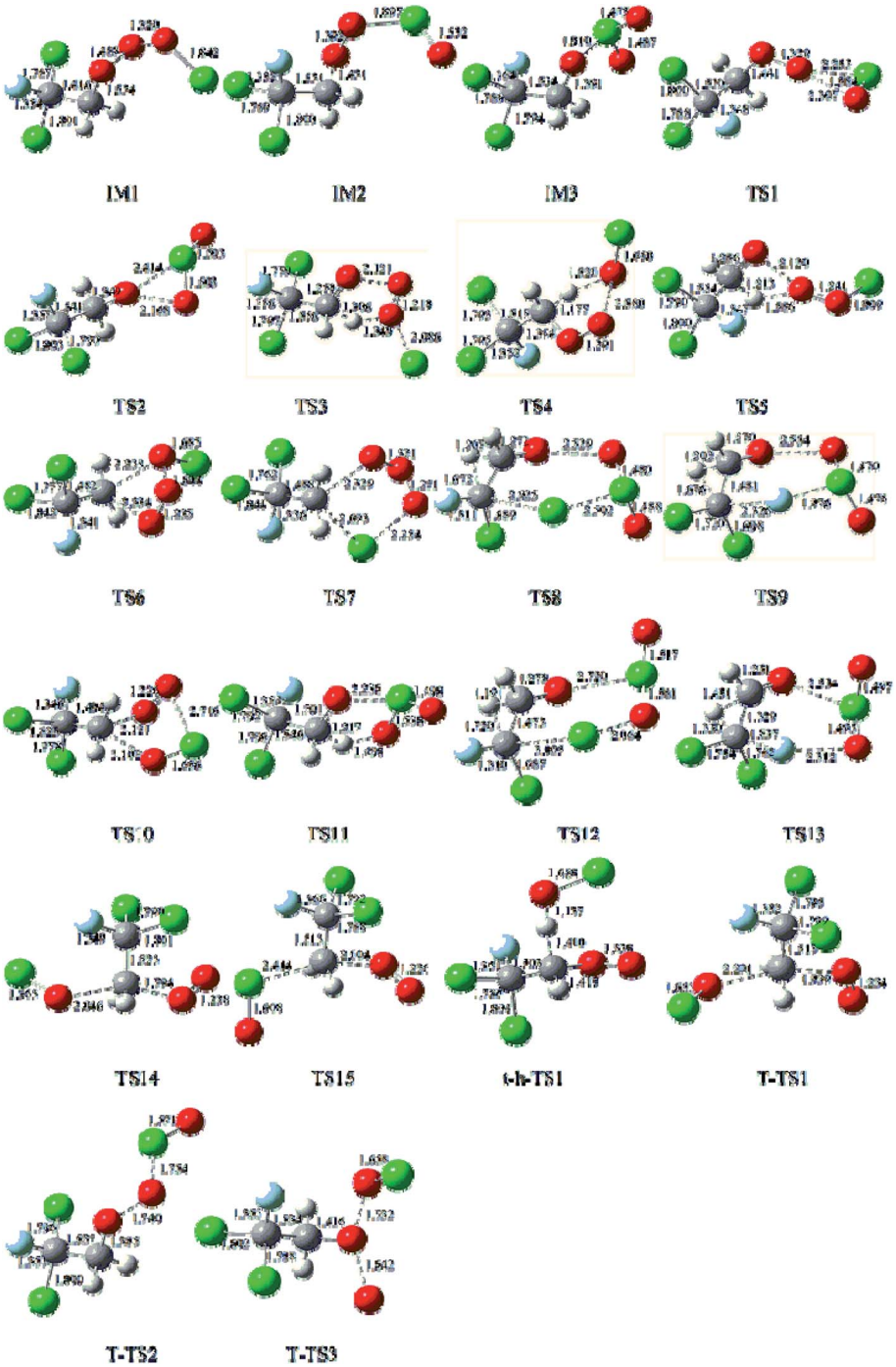

Fig. 1 Optimized geometries for all the intermediates and transition states at the B3LYP/6-311++G(d,p) level for the reaction between $CFCl_2CH_2O_2$ and ClO. Bond distances are given in Å.

undergo the same pathways as that of the $CFCl_2CH_2O_2$ + Cl reaction. Therefore, the aim of the present theoretical investigation is to provide the mechanism and kinetics of the reaction between ClO and $CFCl_2CH_2O_2$ through a description of the potential energy surfaces by means of density functional theory (DFT) theory and RRKM theory,[16] which has been employed to address the complex reactions successfully,[17–22] and shed light on future experimental research.

2. Computational methods

All the geometries were fully optimized using the B3LYP[23,24]/6-311++G(d,p) method. All stationary points were identified for local minima and transition states by vibrational analysis, and connections of the transition states between designated reactants and products were confirmed by intrinsic reaction coordinate (IRC) calculations.[25,26] The energies for the singlet and triplet potential energy surfaces (PES) were refined by the single

point calculations using the CCSD(T)[27]//cc-pVTZ method. Initially obtained PES information, involving optimum geometries, frequencies, moment of inertia and energies of the dominant reaction pathways, were ready for dynamic calculations. RRKM-TST theory was employed to gain the rate constants over a wide temperature and pressure region (200–3000 K and 10^{-14} to 10^{14} torr). The Gaussian 09 program[28] was used to perform the density functional calculations, and Fortran code was used for the RRKM calculations based on the density functional data.

3. Results and discussion

The optimized geometries of all the stationary points involved on the triplet and singlet PESs in the title reaction at the B3LYP/6-311++G(d,p) level are depicted in Fig. 1 and 2, along

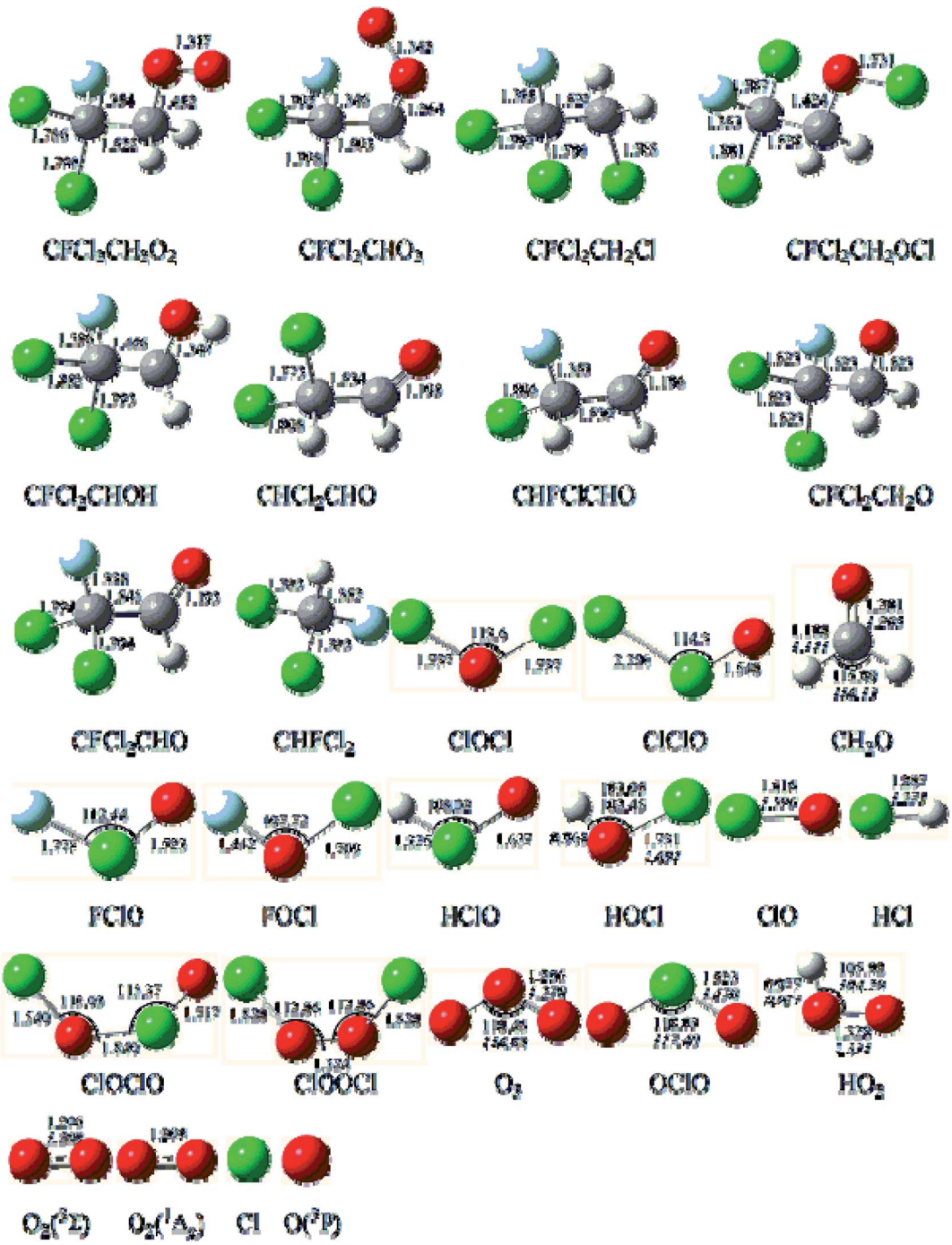

Fig. 2 Optimized geometries (length in Å and angle in degree) for all the reactants and products at the B3LYP/6-311++G(d,p) level for the reaction between $CFCl_2CH_2O_2$ and ClO. Angles are given in °, and bond distances are given in Å. The values in italics are experimental data from ref. 29.

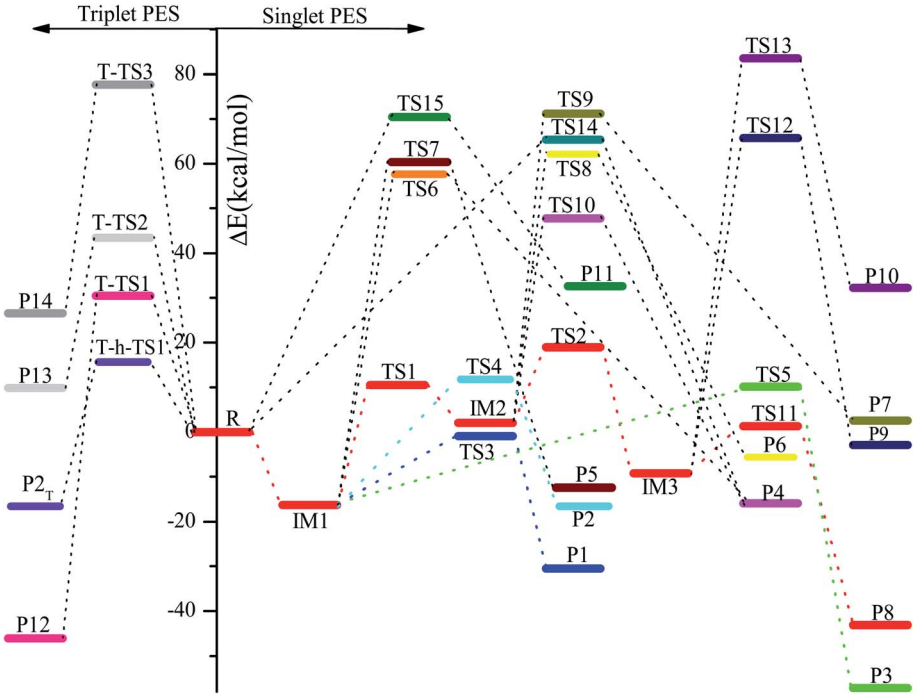

Fig. 3 Potential energy surface obtained at the CCSD(T)//B3LYP level for the $CFCl_2CH_2O_2$ + ClO reaction.

associated with the available experimental values.[29] The frequencies of HOCl, OClO, HO_2, ClO, O_3 and $O_2(^3\Sigma)$ are in agreement with the experimental data (Table S1†). The reaction processes on the singlet and triplet PESs were described clearly, which are represented in Fig. 3. Table 1 summarizes the relative energies (ΔE), relative enthalpies (ΔH), Gibbs free energies (ΔG), and the ZPE for all the stationary points. Table 2 lists the excitation energy (T_V), wavelength (λ) and oscillator strength (f) of the obtained intermediates. The harmonic vibrational frequencies of all the intermediates and transition states found on the PESs are listed in Table S1 as ESI.†

3.1. Generation of adducts on the singlet PES

The generation of the initial adduct involves the addition process of ClO to $CFCl_2CH_2O_2$, which could be described as the approach of the O atom of ClO to the terminal-O atom of $CFCl_2CH_2O_2$ along the O–O reaction coordinate, resulting in the **IM1** ($CFCl_2CH_2OOOCl$) intermediate. Since ClO and $CFCl_2CH_2O_2$ are both radicals, the first association step is expected to be a barrierless process. Moreover, the relaxed scan along the reactive O–O bond confirmed that the first step is a barrierless process. The forming O–O bond is 1.320 Å, and the O–O bond energy is calculated to be 16.28 kcal mol^{-1}. The intermediate **IM1** ($CFCl_2CH_2OOOCl$) can overcome the **TS1** barrier, resulting in **IM2** ($CFCl_2CH_2OOClO$), where the terminal Cl atom is shifted to the middle-O atom of the –OOO– skeleton, and the O–O bond is broken simultaneously. The breaking O–O bond in the triangle structure **TS1** is elongated to 2.307 Å and the forming Cl–O bond is 2.253 Å. The energy barrier for the rearrangement **IM1** ($CFCl_2CH_2OOOCl$) → **TS1** → **IM2** ($CFCl_2CH_2OOClO$) is 26.83 kcal mol^{-1}. The conformer **IM2** ($CFCl_2CH_2OOClO$) can easily isomerize to a minimum energy **IM3** ($CFCl_2CH_2OClO_2$), resulting from the –ClO group shifting to the middle-O atom of the –COO– skeleton, while the O–O bond is broken. The breaking O–O bond in the triangle structure **TS2** is elongated to 2.168 Å and the forming Cl–O bond is 2.414 Å. The energy barrier for **IM2** ($CFCl_2CH_2OOClO$) → **TS2** → **IM3** ($CFCl_2CH_2OClO_2$) is 16.87 kcal mol^{-1}. It should be noted that several conformers for **IM1**, **IM2** and **IM3** exist. We used the lowest-energy conformers in the following discussion. To summarize, three adducts **IM1** ($CFCl_2CH_2OOOCl$), **IM2** ($CFCl_2CH_2OOClO$) and **IM3** ($CFCl_2CH_2OClO_2$) are generated on the singlet PES with the energy of −16.28, 2.05 and −9.21 kcal mol^{-1}, which can further generate many products by isomerization or dissociation before being quenched by collisions, as will be discussed below.

3.2. Decomposition pathways from IM1 ($CFCl_2CH_2OOOCl$), IM2 ($CFCl_2CH_2OOClO$) and IM3 ($CFCl_2CH_2OClO_2$)

Starting from **IM1** ($CFCl_2CH_2OOOCl$), five dissociation pathways were identified. Three intramolecular H-migration channels can be competitive as they possess low barriers and generate stable products. 1,4-H migration from the $–CH_2$ group to the middle-O atom of the –OOCl skeleton, respectively associated with breaking the O–O and O–Cl bonds or O–O bond through **TS3** or **TS4**, gives rise to **P1** ($CFCl_2CHO$ + HO_2 + Cl) or **P2** ($CFCl_2CHO_2$ + HOCl). In **TS3**, the breaking C–H bond (1.306 Å), O–O bond (2.121 Å) and the O–Cl (2.086 Å) bond are elongated by 0.217, 0.633 and 0.244 Å, compared to the intermediate **IM1** ($CFCl_2CH_2OOOCl$) (1.089, 1.488 and 1.842 Å, respectively), and the forming O–H bond is 1.349 Å. In **TS4**, the breaking C–H bond (1.177 Å) and the O–O bond (2.580 Å) are elongated by 0.088 and 1.260 Å, and the forming

Table 1 Zero point energies (ZPE), relative energies (ΔE), relative enthalpies (ΔH) and Gibbs free energy (ΔG) for the species involved in the $CFCl_2CH_2O_2$ + ClO reaction (energies in kcal mol^{-1})

Species	ZPE[a]	ΔE^b	ΔH^b	ΔG^b
R: ($CFCl_2CH_2O_2$+ClO)	29.16	0.00	0.00	0.00
IM1: ($CFCl_2CH_2OOOCl$)	30.87	−16.28	−16.80	−5.03
IM2: ($CFCl_2CH_2OOClO$)	30.57	2.05	1.78	12.98
IM3: ($CFCl_2CH_2OClO_2$)	31.21	−9.21	−9.86	2.58
TS1	30.47	10.55	9.87	21.75
TS2	29.48	18.92	18.28	30.16
TS3	27.56	−0.86	−1.52	10.86
TS4	28.18	11.83	11.32	23.16
TS5	27.62	10.14	9.53	21.59
TS6	28.32	57.61	57.44	68.94
TS7	28.85	60.36	60.08	71.35
TS8	26.91	62.12	62.34	72.17
TS9	26.64	71.16	71.22	82.02
TS10	29.08	47.83	47.45	59.43
TS11	28.36	1.31	0.40	13.64
TS12	26.28	65.73	66.12	75.21
TS13	25.94	83.48	83.50	94.69
TS14	28.57	65.35	65.18	76.82
TS15	28.09	70.47	70.65	80.62
T-h-TS1	25.54	15.73	15.68	25.48
T-TS1	27.95	30.48	30.76	39.18
T-TS2	28.36	43.44	43.33	53.43
T-TS3	28.47	77.65	77.58	87.59
P1: ($CFCl_2CHO$ + HO_2 + Cl)	27.38	−30.48	−29.60	−38.33
P2: (or $\mathbf{P2}_T$): ($CFCl_2CHO_2$ + HOCl)	28.62	−16.54	−16.42	−16.14
P3: ($CFCl_2CHO$ + HOOCl)	29.14	−57.22	−57.30	−57.48
P4: ($CFCl_2CH_2OCl$ + $O_2(^1\Delta_g)$)	29.55	−15.86	−15.76	−13.84
P5: ($CFCl_2CH_2Cl$ + O_3)	29.56	−12.43	−12.79	−11.94
P6: ($CHFClCHO$ + Cl_2O_2)	29.64	−5.61	−5.84	−6.37
P7: ($CHCl_2CHO$ + $FClO_2$)	29.31	2.55	2.26	1.98
P8: ($CFCl_2CHO$ + HOClO)	28.53	−43.06	−43.04	−43.41
P9: ($CHFClCHO$ + ClOClO)	28.48	−2.86	−2.75	−4.16
P10: ($CHCl_2CHO$ + FOClO)	27.98	32.26	32.36	31.13
P11: ($CFCl_2CH_2ClO$ + $O_2(^1\Delta_g)$)	28.33	32.58	32.94	34.01
P12: ($CFCl_2CH_2OCl$ + $O_2(^3\Sigma)$)	29.57	−46.01	−45.92	−44.64
P13: ($CFCl_2CH_2O$ + OClO)	27.77	9.88	9.63	9.19
P14: ($CFCl_2CH_2OOCl$ + $O(^3P)$)	29.04	26.55	26.76	29.80

[a] At the B3LYP/6-311++G(d,p) level. [b] The relative energies are calculated at the CCSD(T)/cc-pVTZ + ZPE level.

O–H bond is 1.520 Å. Alternatively, 1,3-H migration from the $–CH_2$ group to the middle-O atom of the –OOO– skeleton in **IM1**, along with breakage of the O–O bond *via* **TS5**, results in **P3** ($CFCl_2CHO$ + HOOCl). The above three decomposition channels need to overcome 15.42, 28.11 and 26.42 kcal mol^{-1} energy barriers, respectively. The overall exothermicities of generating the **P1** ($CFCl_2CHO$ + HO_2 + Cl), **P2** ($CFCl_2CHO_2$ + HOCl) and **P3** ($CFCl_2CHO$ + HOOCl) channels are estimated to be 29.60, 16.42 and 57.30 kcal mol^{-1}, respectively, implying that the most significant reaction pathway is the generation of **P1** ($CFCl_2CHO$ + HO_2 + Cl), and the pathways to generate **P2** ($CFCl_2CHO_2$ + HCl) and **P3** ($CFCl_2CHO$ + HOOCl) compete with each other.

When we considered the other direct dissociation channels from **IM1** ($CFCl_2CH_2OOOCl$), one four-center and five-center transition state (**TS6** and **TS7**) were identified. **TS6** connects the **IM1** ($CFCl_2CH_2OOOCl$) and **P4** ($CFCl_2CH_2OCl$ + $O_2(^1\Delta_g)$) end products, whereas **P5** ($CFCl_2CH_2Cl$ + O_3) is generated from **IM1** ($CFCl_2CH_2OOOCl$) passing through **TS7**. These two channels can be attributed to the –ClO group or terminal-Cl atom shifting to the carbon atom, and the $O_2(^1\Delta_g)$ or O_3 leaving simultaneously, respectively. **TS6** and **TS7**, with imaginary frequencies of 386i and 439i cm^{-1}, respectively, are first-order saddle points, which was confirmed by vibrational frequency analysis. The energy barriers of **IM1** ($CFCl_2CH_2OOOCl$) → **TS6** → **P4** ($CFCl_2CH_2OCl$ + $O_2(^1\Delta_g)$) and **IM1** ($CFCl_2CH_2OOOCl$) → **TS7** → **P5** ($CFCl_2CH_2Cl$ + O_3) are 73.89 and 76.64 kcal mol^{-1}. Thus, neither the $O_2(^1\Delta_g)$ or O_3 elimination channels from **IM1** are favorable judging from the high barrier height.

Two elimination mechanisms were located from **IM2** ($CFCl_2CH_2OOClO$) through a dicyclo-transition state **TS8** or **TS9** to generate **P6** ($CHFClCHO$ + Cl_2O_2) or **P7** ($CHCl_2CHO$ + $FClO_2$); this occurred through one of the H atoms in the $–CH_2$ group migrating to another carbon atom, and one of the Cl atoms or F atom in the $-CFCl_2$ group shifting to the Cl atom in the –OOClO skeleton, accompanied by the O–O bond breaking. The breaking C–H, C–Cl and O–O bonds are elongated to 1.207, 2.925 and 2.529 Å, and the forming C–H and Cl–Cl bond are 1.672 and 2.502 Å for **TS8**. The breaking C–H, C–F and O–O bonds are elongated to 1.202, 2.326 and 2.554 Å, and the forming C–H and F–Cl bonds are 1.676 and 1.976 Å for **TS9**. Vibrational frequency analysis of **TS8** and **TS9** reveals one imaginary frequency of 661*i* and 699*i* cm^{-1}, respectively. The activation barriers for **IM2** ($CFCl_2CH_2OOClO$) → **TS8** → **P6** ($CHFClCHO$ + Cl_2O_2) and **IM2** ($CFCl_2CH_2OOClO$) → **TS9** → **P7** ($CHCl_2CHO$ + $FClO_2$) are 60.07 and 69.11 kcal mol^{-1}. The high

Table 2 The excitation energy T_V (in eV), oscillator strength f (in atomic units) and wavelength λ (in nm) of the first five excited states of **IM1** ($CFCl_2CH_2OOOCl$), **IM2** ($CFCl_2CH_2OOClO$) and **IM3** ($CFCl_2CH_2OClO_2$) at the TD-B3LYP level of theory

	IM1 ($CFCl_2CH_2OOOCl$)			**IM2** ($CFCl_2CH_2OOClO$)			**IM3** ($CFCl_2CH_2OClO_2$)		
Excited states	T_V	f	λ	T_V	f	λ	T_V	f	λ
1	3.01	0.0001	411.6	1.98	0.0000	625.59	3.48	0.0016	356.4
2	4.07	0.0001	304.7	3.47	0.0015	357.27	4.31	0.0641	287.3
3	5.02	0.0371	247.1	4.42	0.2574	280.47	4.67	0.0015	265.4
4	5.12	0.0201	242.1	4.69	0.0004	263.91	5.61	0.0663	221.0
5	5.72	0.1630	216.8	5.57	0.0013	222.45	5.71	0.0611	217.0

barriers restrain these two dissociation pathways from proceeding.

We also considered the dissociation pathway from **IM2** ($CFCl_2CH_2OOClO$) resulting in the **P4** ($CFCl_2CH_2OCl + O_2(^1\Delta_g)$) products, and transition state **TS10** was located for this channel. **TS10** is a COOClO five-center transition state, that involves the C–O and Cl–O bonds breaking and forming another C–O bond, accompanied with the dissociation of $O_2(^1\Delta_g)$. The energy barrier is 45.78 kcal mol^{-1}, suggesting that the conversion of **IM2** ($CFCl_2CH_2OOClO$) → **TS10** → **P4** ($CFCl_2CH_2OCl + O_2(^1\Delta_g)$) was inefficient.

IM3 ($CFCl_2CH_2OClO_2$) involves a 1,4-H shift from the carbon atom of the $-CH_2$ group to the oxygen atom, along with breakage of the O–Cl bond leading to **P8** ($CFCl_2CHO + HOClO$) *via* **TS11**. **TS11** presents a non-planar and loose HCOClO five-membered ring structure with long C–H, O–Cl and O–H distances, that is, r(C–H) = 1.217 Å, r(O–Cl) = 2.238 Å, and r(O–H) = 1.498 Å. The **IM3** ($CFCl_2CH_2OClO_2$) → **TS11** → **P8** ($CFCl_2CHO + HOClO$) transformation barrier is 10.52 kcal mol^{-1} and **TS11** is only 1.31 kcal mol^{-1} higher than the reactants. Therefore, this dissociation pathway may be important for the reaction.

IM3 ($CFCl_2CH_2OClO_2$) could also undergo a respective 1,5-Cl shift or 1,5-F shift from the carbon atom to the oxygen atom, and a 1,2-H shift from the carbon atom of the $-CH_2$ group to another carbon atom as well, which is associated with breaking the O–Cl bond (*i.e.*, **TS12** and **TS13** together generate product **P9** ($CHFClCHO + (ClO)_2$) and **P10** ($CHCl_2CHO + FOClO$)). The loose ClCCOClO and FCCOClO six-membered rings are nonplanar and found in **TS12** and **TS13**, respectively. In **TS12**, the breaking C–H, C–Cl and O–Cl bonds and the forming C–H and Cl–O bonds are 1.191, 3.005, 2.720, 1.720 and 2.064 Å, respectively. In **TS13**, the C–H, C–F and O–Cl bonds that will be broken and the C–H and F–O bond that will be formed are 1.451, 1.837, 2.534, 1.330 and 2.312 Å, respectively. The decomposition barriers of **IM3** ($CFCl_2CH_2OClO_2$) → **TS12** → **P9** ($CHFClCHO + (ClO)_2$) and **IM3** ($CFCl_2CH_2OClO_2$) → **TS13** → **P10** ($CHCl_2CHO + FOClO$) are 74.94 and 92.69 kcal mol^{-1}, which are quite high, making the generation of **P9** ($CHFClCHO + (ClO)_2$) and **P10** ($CHCl_2CHO + FOClO$) highly impossible.

3.3. S_N2 displacement pathways on the singlet PES

Another type of mechanism (S_N2 displacement reaction) could take place for the $CFCl_2CH_2O_2 + ClO$ reaction. Two different transition states were identified. The two S_N2 displacement channels can be attributed to the O atom or the Cl atom in ClO respectively attacking the C atom of the $-CH_2$ group in CH_3CFClO_2, along with the $O_2(^1\Delta_g)$ group leaving *via* **TS14** or **TS15**, leading to **P4** ($CFCl_2CH_2OCl + O_2(^1\Delta_g)$) or **P11** ($CFCl_2CH_2ClO + O_2(^1\Delta_g)$). The forming and breaking C–O bonds in **TS14** and the forming C–Cl bond and breaking C–O bond in **TS15** are respectively 2.046, 1.794 Å, and 2.414, 2.004 Å. The processes of R → **TS14** → **P4** ($CFCl_2CH_2OCl + O_2(^1\Delta_g)$) and R → **TS15** → **P11** ($CFCl_2CH_2ClO + O_2(^1\Delta_g)$) require quite high energy barriers of 65.35 and 70.47 kcal mol^{-1}. Thus, these two S_N2 displacement channels are prohibited kinetically.

3.4. The pathways on the triplet PES

On the triplet surface, both H-abstraction and S_N2 displacement reaction mechanisms were identified. Surmounting **T-h-TS1**, **T-TS1**, **T-TS2** and **T-TS3**, **P2$_T$** ($CFCl_2CHO_2 + HCl$), **P12** ($CFCl_2CH_2OCl + O_2(^3\Sigma)$), **P13** ($CFCl_2CH_2O + OClO$) and **P14** ($CFCl_2CH_2OOCl + O(^3P)$) are produced, and the relative energy is −16.54, −46.01, 9.88 and 26.55 kcal mol^{-1}, respectively. The barriers of these four channels are 15.73, 30.48, 43.44 and 77.65 kcal mol^{-1}, respectively. Compared with the addition/elimination pathways on the singlet PES, the pathways on the triplet PES are energetically less convenient because of the higher barrier heights.

3.5. RRKM-TST calculations of the rate constants

Because the energy barriers are much higher than the obtained dominant pathways (Scheme 1), we ignore the pathways to produce **P4** ($CFCl_2CH_2OCl + O_2(^1\Delta_g)$), **P5** ($CFCl_2CH_2Cl + O_3$), **P6** ($CHFClCHO + Cl_2O_2$), **P7** ($CHCl_2CHO + FClO_2$), **P9** ($CHFClCHO + (ClO)_2$), **P10** ($CHCl_2CHO + FOClO$), **P11** ($CFCl_2CH_2ClO + O_2\ (^1\Delta_g)$), **P12** ($CFCl_2CH_2OCl + O_2(^3\Sigma)$), **P13** ($CFCl_2CH_2O + OClO$) and **P14** ($CFCl_2CH_2OOCl + O(^3P)$) in the RRKM calculations. The predicted rate constants of **IM1** ($CFCl_2CH_2OOOCl$), **IM2** ($CFCl_2CH_2OOClO$), **IM3** ($CFCl_2CH_2OClO_2$), **P1** ($CFCl_2CHO + HO_2 + Cl$), **P2** ($CFCl_2CHO_2 + HOCl$), **P3** ($CFCl_2CHO + HOOCl$), and **P8** ($CFCl_2CHO + HOClO$) are denoted as k_{IM1}, k_{IM2}, k_{IM3}, k_{P1}, k_{P2}, k_{P3} and k_{P8}, and the total rate constant is denoted as $k_{tot} = k_{IM1} + k_{IM2} + k_{IM3} + k_{P1} + k_{P2} + k_{P3} + k_{P8}$ at 200–3000 K, 12 torr N_2, which are presented in Fig. 4. The estimated values of k_{tot} are consistent with the experimental data (*e.g.* $k_{tot} = 6.39 \times 10^{-12}$ cm^3 per molecule per s *vs.* 6.70×10^{-12} cm^3 per molecule per s at 298 K). k_{tot} appears to decrease first and then increase as the temperature increases. The branching ratios are presented Fig. S1.† The low-

SCHEME 1

$CFCl_2CH_2O_2+ClO \longrightarrow IM1(CFCl_2CH_2OOOCl) \longrightarrow P1(CFCl_2CHO + HO_2 + Cl)$

$\longrightarrow P2(CFCl_2CHO_2 + HOCl)$

$\longrightarrow P3(CFCl_2CHO + HOOCl)$

$\longrightarrow IM2(CFCl_2CH_2OOClO) \longrightarrow IM3(CH_3CH_2OClO_2) \longrightarrow P8(CFCl_2CHO+HOClO)$

Scheme 1 The primary pathways of the $CFCl_2CH_2O_2 + ClO$ reaction.

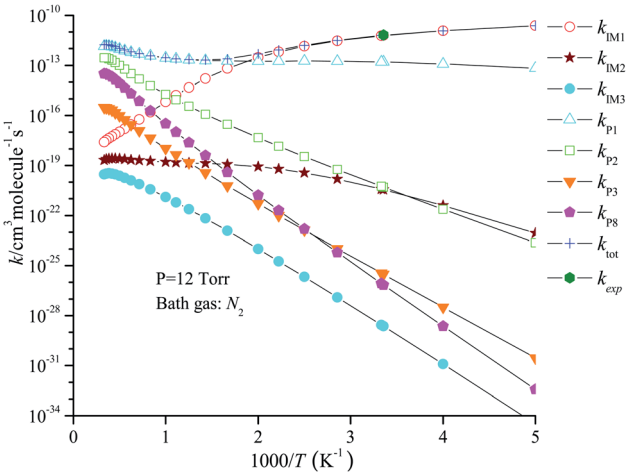

Fig. 4 Plots of the rate coefficients for total and primary reaction channels *versus* 1000/T (K^{-1}) at 200–1000 K associated with the available experimental value.

temperature (200–500 K) association is dominated by the production of **IM1** ($CFCl_2CH_2OOOCl$), and the production of **P1** ($CFCl_2CHO + HO_2 + Cl$) quickly becomes dominant with the rise of temperature (500–3000 K). The **P2** ($CFCl_2CHO_2 + HOCl$) product channel contributes to the reaction at $T > 1200$ K. The **P3** ($CFCl_2CHO + HOOCl$) product pathway generating from **IM1** ($CFCl_2CH_2OOOCl$), the **P8** ($CFCl_2CHO + HOClO$) product pathway generating from **IM3** ($CFCl_2CH_2OClO_2$) and the pathways of the **IM2** ($CFCl_2CH_2OOClO$) and **IM3** ($CFCl_2CH_2OClO_2$) collisional stabilization rarely occur at any temperature.

The rate constants for the generation of branched products of the $ClO + CFCl_2CH_2O_2$ reaction at different pressures are shown in Fig. 5. Due to the competition between decomposition and stabilization, k_{IM1}, k_{IM2} and k_{IM3} are for the generation of **IM1**, **IM2** and **IM3** by collisional deactivation, and k_{P1}, k_{P2}, k_{P3} and k_{P8} are for the generation of **P1**, **P2**, **P3** and **P8**, which demonstrate strong dependence on pressure. The pattern of the pressure dependence of **IM1** (10^{-10} to 10^{10} atm), **IM2** (10^{-10} to 10^{2} atm) and **IM3** (10^{-10} to 10^{2} atm) is contrary to the dissociation process and **IM2** (10^{2} to 10^{10} atm) and **IM3** (10^{2} to 10^{10} atm). k_{IM1}, k_{IM2} and k_{IM3} are very small and not competitive at lower pressure; when the pressure exceeds 10^{-4} atm, k_{IM1} is near the high pressure limit at $T > 1000$ K. In addition, k_{IM1} displays strong negative dependence on temperature at 200–3000 K, owing to the reduction of the collision inactivation rate. The rate constants for the dissociation procedure k_{P1} display positive dependence on temperature and negative dependence on pressure. At low temperatures and high pressures, k_{P1}, k_{P2}, k_{P3} and k_{P8} become negligible.

The branching ratios of the individual product pathways of the $CFCl_2CH_2O_2 + ClO$ reaction at the low pressure limit (10^{-10}

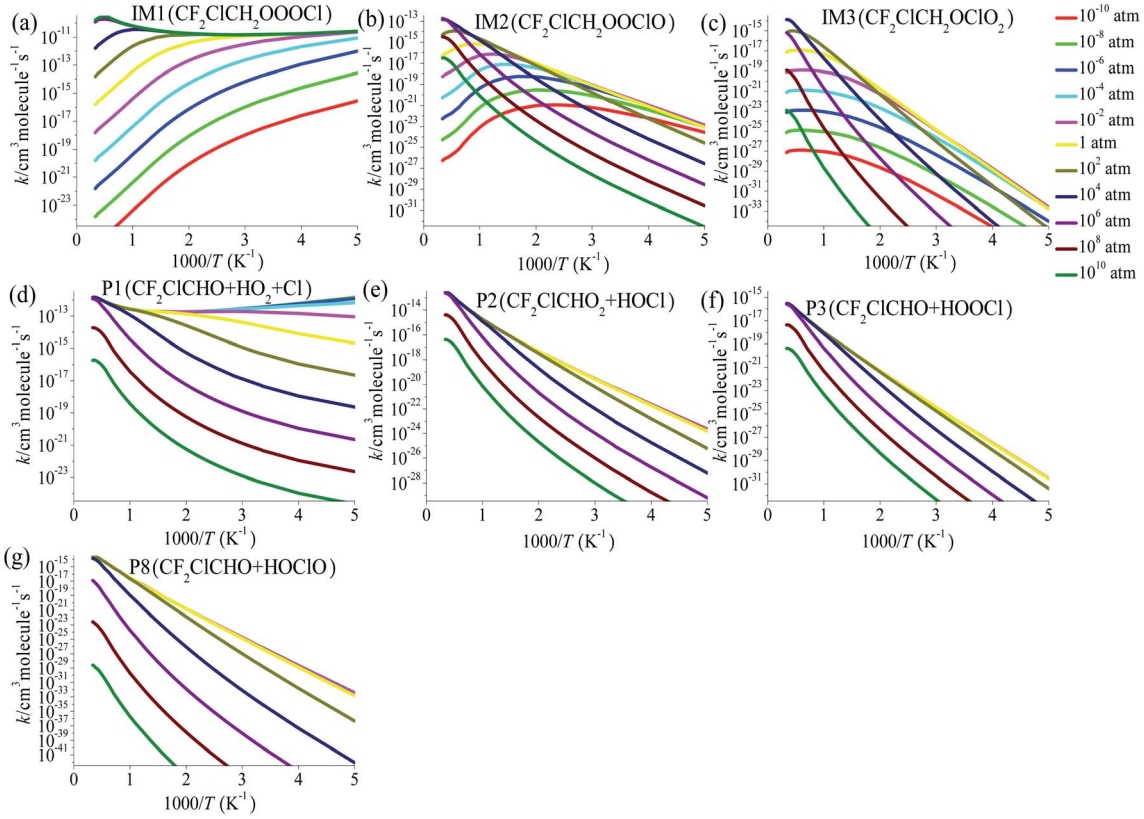

Fig. 5 Predicted rate coefficients for the total reaction and each individual product pathway of the reaction between $CFCl_2CH_2O_2$ and ClO at 200–3000 K and 10^{-10} to 10^{10} atm.

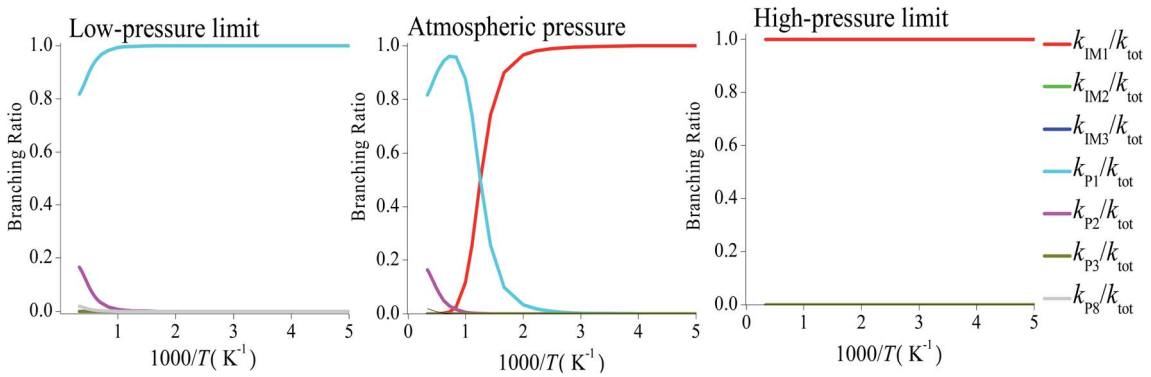

Fig. 6 Predicted branching ratios for the $CFCl_2CH_2O_2$ + ClO reaction at the low pressure limit, atmospheric pressure and high pressure limit.

atm), atmospheric pressure (1 atm) and high pressure limit (10^{10} atm) are presented in Fig. 6. Seven primary product pathways dominate noticeably – the competitive inactivation and dissociation that generate **IM1**, **IM2**, **IM3**, **P1**, **P2**, **P3** and **P8**, respectively. At the low and high pressure limits, the production of **P1** ($CFCl_2CHO$ + HO_2 + Cl) and **IM1** ($CFCl_2CH_2OOOCl$) predominate the reaction at 200–3000 K, respectively. At atmospheric pressure and high temperatures, the generation of **P1** ($CFCl_2CHO$ + HO_2 + Cl) dominates the reaction; conversely, at moderate and low temperatures, the collision inactivation of **IM1** ($CFCl_2CH_2OOOCl$) takes over the reaction.

The three-parameter Arrhenius equations for the rate constants of generating **IM1** ($CFCl_2CH_2OOOCl$) (k_{IM1}) and **P1** ($CFCl_2CHO$ + HO_2 + Cl) (k_{P1}) at the low pressure limit, atmospheric pressure and high pressure limit of N_2 can be represented by:

$$k^0_{IM1}(CFCl_2CH_2OOOCl)/(cm^3 \text{ per molecule per s}) = 4.23 \times 10^{-23} T^{-4.13} \exp(7517.87/T) \quad (200 \le T \le 3000\ K)$$

$$k^0_{P1}(CFCl_2CHO + HO_2 + Cl)/(cm^3 \text{ per molecule per s}) = 1.01 \times 10^{-16} T^{0.85} \exp(1001.83/T) \quad (200 \le T \le 500\ K)$$
$$= 9.45 \times 10^{-15} T^{0.69} \exp(-1327.18/T) \quad (500 < T \le 3000\ K)$$

$$k_{IM1}(CFCl_2CH_2OOOCl)/(cm^3 \text{ per molecule per s}) = 1.84 \times 10^{-7} T^{-1.72} \exp(62.58/T) \quad (200 \le T \le 3000\ K)$$

$$k_{P1}(CFCl_2CHO + HO_2 + Cl)/(cm^3 \text{ per molecule per s}) = 2.38 \times 10^{-15} T^{0.85} \exp(-990.60/T) \quad (200 \le T \le 3000\ K)$$

$$k^\infty_{IM1}(CFCl_2CH_2OOOCl)/(cm^3 \text{ per molecule per s}) = 5.43 \times 10^{-18} T^{2.36} \exp(47.22/T) \quad (200 \le T \le 1800\ K)$$
$$= 1.08 \times 10^{-9} T^{-0.33} \exp(2682.26/T) \quad (1800 < T \le 3000\ K)$$

$$k^\infty_{P1}(CFCl_2CHO + HO_2 + Cl)/(cm^3 \text{ per molecule per s}) = 1.14 \times 10^{-10} T^{-1.30} \exp(8395.50/T) \quad (200 \le T \le 3000\ K)$$

We also examined the pressure effect of the total rate constants at selected low (298 K), moderate (500 K and 1000 K),

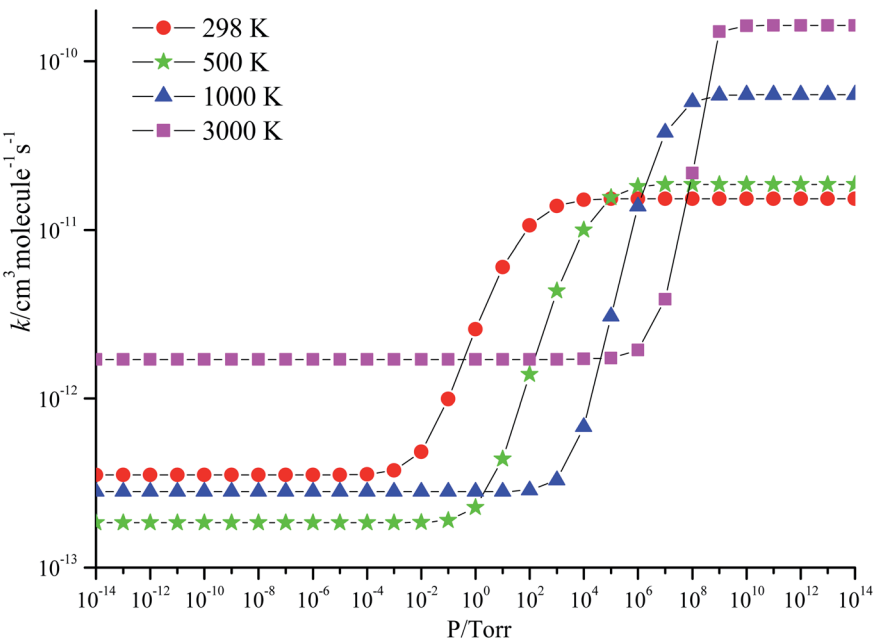

Fig. 7 Pressure dependence of the total rate coefficients for the $CFCl_2CH_2O_2$ + ClO reaction at 298, 1000 and 3000 K.

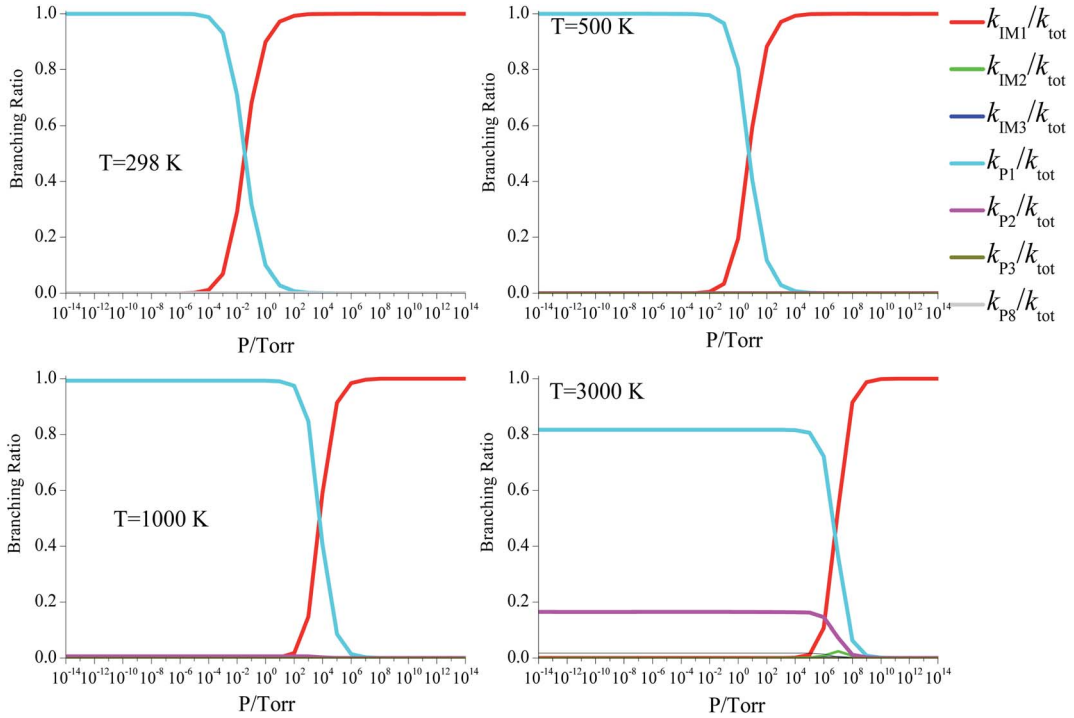

Fig. 8 Branching ratios for the $CFCl_2CH_2O_2$ + ClO reaction at 10^{-14} to 10^{14} torr at 298, 1000 and 3000 K.

and high (3000 K) temperatures (Fig. 7), and established the branching ratios of the individual product pathways of the $CFCl_2CH_2O_2$ + ClO reaction (Fig. 8). Fig. 7 displays the typical "S" behavior, and the "S" region moves to the high pressure range as the temperature increases. The "S" regions are 10^{-4} to 10^{4}, 10^{-1} to 10^{6}, 10^{2}–10^{9} and 10^{5}–10^{10} torr at selected temperatures, respectively. At each respective temperature, the branching ratio for **P1** ($CFCl_2CHO$ + HO_2 + Cl) (k_{P1}/k_{tot}) possesses the largest values in the pressure ranges of 10^{-14} to 10^{-2}, 10^{-14} to 10^{1}, 10^{-14} to 10^{4}, and10^{-14} to 10^{7} torr, respectively. But at higher pressures, the branching ratio for the energized **IM1** ($CFCl_2CH_2OOOCl$) intermediate, which is stabilized by collisions, becomes dominant.

3.6. Atmospheric lifetimes of $CFCl_2CH_2O_2$

The atmospheric lifetime of $CFCl_2CH_2O_2$ can be deduced by the following formula:$\tau = \frac{1}{k[ClO]}$. The calculated average daytime atmospheric concentration of chlorine monoxide radical (ClO) is 1×10^{7} molecules per cm^3 (Tang, 2004),[30] and $k_{ClO} = 1.36 \times 10^{-11}$ cm^3 per molecule per s was estimated. The atmospheric lifetime of $CFCl_2CH_2O_2$ is approximately 2.04 h, which suggests that the ClO-initiated reaction with $CFCl_2CH_2O_2$ plays an important role in some special areas and the marine boundary layer.

3.7. Vertical excitation energy of IM1 ($CFCl_2CH_2OOOCl$), IM2 ($CFCl_2CH_2OOClO$) and IM3 ($CFCl_2CH_2OClO_2$)

The photo-oxidation of compounds containing chlorine is significant for Cl atmospheric chemistry and might influence the stratosphere and troposphere. To gain new insight into the photolytic stability of the Cl-containing compounds, the vertical excitation energy (T_V) of the first five excited states for **IM1** ($CFCl_2CH_2OOOCl$), **IM2** ($CFCl_2CH_2OOClO$) and **IM3** ($CFCl_2CH_2OClO_2$) were calculated by TDDFT employing B3LYP/6-311++G(d,p), and the results, including wavelength (λ), excitation energy (T_V) and oscillator strength (f), are listed in Table 2. Compounds will typically photolyze if the T_V value is smaller than 4.13 eV or the wavelength is longer than 300 nm. It is seen from Table 2 that the T_V value of the first two excited states of **IM1** ($CFCl_2CH_2OOOCl$) are 3.01 eV (411.6 nm) and 4.07 eV (304.7 nm) and the oscillator strengths are 0.0001 and 0.0001; the second excited state of **IM2** ($CFCl_2CH_2OOClO$) is 3.47 eV (357.27 nm) and the oscillator strength is 0.0015; the T_V value and oscillator strength of the first excited state of **IM3** ($CFCl_2CH_2OClO_2$) are 3.48 eV (356.4 nm) and 0.0016, respectively, indicating that the photolysis of **IM1** ($CFCl_2CH_2OOOCl$), **IM2** ($CFCl_2CH_2OOClO$) and **IM3** ($CFCl_2CH_2OClO_2$) could occur under sunlight.

4. Conclusions

The ClO-initiated oxidation reaction of $CFCl_2CH_2O_2$ was researched by means of density functional theory (DFT) and RRKM theory to understand the mechanism and product distribution. On the singlet PES, the addition of the O atom of ClO to the terminal-O of $CFCl_2CH_2O_2$ to generate **IM1** ($CFCl_2CH_2OOOCl$) is more favorable at 200–500 K, followed by intramolecular 1,4-H shifts along with breakage of the O–Cl bond to generate **P1** ($CFCl_2CHO$ + HO_2 + Cl), which dominates the reaction at high temperatures. The kinetics simulations revealed that the total rate constants exhibit typical "falloff" behavior. The pathways on the triplet PES are less preferred over

the pathways on the singlet PES. The ClO-determined lifetime of $CFCl_2CH_2O_2$ is 2.04 h. **IM1** ($CFCl_2CH_2OOOCl$), **IM2** ($CFCl_2CH_2OOClO$) and **IM3** ($CFCl_2CH_2OClO_2$) will photolyze under the sunlight.

Conflicts of interest

There are no conflicts to declare.

Acknowledgements

This work was supported by the Natural Science Foundations of China (No. 21707062).

References

1 E. C. Tuazon and R. Atkinson, *Potential Replacements for the Chlorofluorocarbons and Halons*, American Chemical Society, Washington, DC, 1995.
2 J. Sehested, *Int. J. Chem. Kinet.*, 1994, **26**, 1023–1039.
3 R. Atkinson, D. L. Baulch, R. A. Cox, R. F. Hampson Jr, J. A. Kerr, M. J. Rossi and J. Troe, *J. Phys. Chem. Ref. Data*, 1997, **26**, 521–1011.
4 P. D. Lightfoot, R. A. Cox, J. N. Crowley, M. Destriau, G. D. Hayman, M. E. Jenkin, G. K. Moortgat and F. Zabel, *Atmos. Environ., Part A*, 1992, **26**, 1805–1961.
5 T. J. Wallington and O. J. Nielsen, *Int. J. Chem. Kinet.*, 1991, **23**, 785–798.
6 R. W. Carr, D. G. Peterson and F. K. Smith, *J. Phys. Chem.*, 1986, **90**, 607.
7 F. X. Wu and R. W. Carr, *J. Phys. Chem.*, 1995, **99**, 3128–3136.
8 J. Sehested, O. J. Nielsen and T. J. Wallington, *Chem. Phys. Lett.*, 1993, **213**, 457–464.
9 F. X. Wu and R. W. Carr, *Int. J. Chem. Kinet.*, 1996, **28**, 9–19.
10 G. D. Hayman and F. Battin-Leclerc, *J. Chem. Soc., Faraday Trans.*, 1995, **91**, 1313–1323.
11 D. E. Shallcross, M. T. Raventos-Duran, M. W. Bardwell, A. Bacak, Z. Solman and C. J. Percival, *Atmos. Environ.*, 2005, **35**, 763–771.
12 S. Y. Du, J. S. Francisco, G. K. Schenter and B. C. Garrett, *J. Am. Chem. Soc.*, 2009, **131**, 14778–14785.
13 J. G. Anderson, D. Toohey and W. Brune, *Science*, 1991, **251**, 39–46.
14 F. D. Pope, J. C. Hansen, K. D. Bayes, R. R. Friedl and S. P. Sander, *Cheminform*, 2007, **111**, 4322–4332.
15 Y. J. Zhang, B. He and Y. X. Sun, *J. Mol. Graphics Modell.*, 2020, **99**, 107618.
16 K. A. Holbrook, M. J. Pilling, and S. H. Robertson, *Unimolecular Reactions*, J. Wiley, Chichester, UK, 1996.
17 H. Hou, B. S. Wang and Y. S. Gu, *J. Phys. Chem. A*, 2000, **104**, 320.
18 H. Hou and B. S. Wang, *J. Chem. Phys.*, 1999, **103**, 8021–8029.
19 Y. J. Zhang, J. Y. Sun, K. Chao, H. Sun, F. Wang, S. W. Tang, X. M. Pan, J. P. Zhang and R. S. Wang, *J. Phys. Chem. A*, 2012, **116**, 3172.
20 J. Y. Sun, R. S. Wang and B. S. Wang, *Phys. Chem. Chem. Phys.*, 2011, **13**, 16585.
21 S. H. Mousavipour, S. Ramazani and Z. Shahkolahi, *J. Phys. Chem. A*, 2009, **113**, 2838.
22 Y. J. Zhang, K. Chao, J. Y. Sun, Z. M. Su, X. M. Pan, J. P. Zhang and R. S. Wang, *J. Phys. Chem. A*, 2013, **117**, 6629–6640.
23 A. D. Becke, *J. Chem. Phys.*, 1993, **98**, 5648.
24 C. Lee, W. Yang and R. G. Par, *Phys. Rev. B: Condens. Matter Mater. Phys.*, 1988, **37**, 785.
25 C. Gonzalez and H. B. Schlegel, *J. Chem. Phys.*, 1989, **90**, 2154–2161.
26 C. Gonzalez and H. B. Schlegel, *J. Phys. Chem.*, 1990, **94**, 5523–5527.
27 K. Raghavachari, G. W. Trucks, J. A. Pople and M. Head-Gordon, *Chem. Phys. Lett.*, 1989, **157**, 479–483.
28 M. J. Frisch, G. W. Trucks, H. B. Schlegel, G. E. Scuseria, M. A. Robb, J. R. Cheeseman, G. Scalmani, V. Barone, B. Mennucci, G. A. Petersson, H. Nakatsuji, M. Caricato, X. Li, H. P. Hratchian, A. F. Izmaylov, J. Bloino, G. Zheng, J. L. Sonnenberg, M. Hada, M. Ehara, K. Toyota, R. Fukuda, J. Hasegawa, M. Ishida, T. Nakajima, Y. Honda, O. Kitao, H. Nakai, T. Vreven, J. A. Montgomery Jr, J. E. Peralta, F. Ogliaro, M. Bearpark, J. J. Heyd, E. Brothers, K. N. Kudin, V. N. Staroverov, R. Kobayashi, J. Normand, K. Raghavachari, A. Rendell, J. C. Burant, S. S. Iyengar, J. Tomasi, M. Cossi, N. Rega, J. M. Millam, M. Klene, J. E. Knox, J. B. Cross, V. Bakken, C. Adamo, J. Jaramillo, R. Gomperts, R. E. Stratmann, O. Yazyev, A. J. Austin, R. Cammi, C. Pomelli, J. W. Ochterski, R. L. Martin, K. Morokuma, V. G. Zakrzewski, G. A. Voth, P. Salvador, J. J. Dannenberg, S. Dapprich, A. D. Daniels, O. Farkas, J. B. Foresman, J. V. Ortiz, J. Cioslowski and D. J. Fox, Gaussian, Inc, Wallingford CT, 2009.
29 *NIST Computational Chemistry Comparison and Benchmark Database*, http://srdata.nist.gov/cccbdb/.
30 C. T. Chang, T. H. Liu and F. T. Jeng, *Environ. Res.*, 2004, **94**, 67–74.

